Developmental Cell
Article

Robo4 Maintains Vessel Integrity and Inhibits Angiogenesis by Interacting with UNC5B

Alexander W. Koch,[1,4,5,*] Thomas Mathivet,[2,4] Bruno Larrivée,[2] Raymond K. Tong,[1] Joe Kowalski,[1] Laurence Pibouin-Fragner,[2] Karine Bouvrée,[2] Scott Stawicki,[1] Katrina Nicholes,[1] Nisha Rathore,[1] Suzie J. Scales,[1] Elizabeth Luis,[1] Raquel del Toro,[2] Catarina Freitas,[2] Christiane Bréant,[2] Annie Michaud,[2] Pierre Corvol,[2] Jean-Léon Thomas,[3] Yan Wu,[1] Franklin Peale,[1] Ryan J. Watts,[1] Marc Tessier-Lavigne,[1] Anil Bagri,[1] and Anne Eichmann[2,6,7,*]

[1]Genentech Inc., South San Francisco, CA 94030, USA
[2]Inserm U833, Collège de France, 75005 Paris, France
[3]Inserm UMR-S 975, CNRS UMR 7225, UPMC, Hôpital de la Salpêtrière, 75013 Paris, France
[4]These authors contributed equally to this work
[5]Present address: Novartis Institutes for BioMedical Research, Inc., 100 Technology Square, Cambridge, MA 02139, USA
[6]Present address: CIRB Collège de France/CNRS UMR 7241/INSERM U1050
[7]Present address: Department of Cardiology, Yale University School of Medicine, 300 George Street, New Haven, CT 06510-3221, USA
*Correspondence: alexander.koch@novartis.com (A.W.K.), anne.eichmann@college-de-france.fr (A.E.)
DOI 10.1016/j.devcel.2010.12.001

SUMMARY

Robo4 is an endothelial cell-specific member of the Roundabout axon guidance receptor family. To identify Robo4 binding partners, we performed a protein-protein interaction screen with the Robo4 extracellular domain. We find that Robo4 specifically binds to UNC5B, a vascular Netrin receptor, revealing unexpected interactions between two endothelial guidance receptors. We show that Robo4 maintains vessel integrity by activating UNC5B, which inhibits signaling downstream of vascular endothelial growth factor (VEGF). Function-blocking monoclonal antibodies against Robo4 and UNC5B increase angiogenesis and disrupt vessel integrity. Soluble Robo4 protein inhibits VEGF-induced vessel permeability and rescues barrier defects in *Robo4*$^{-/-}$ mice, but not in mice treated with anti-UNC5B. Thus, Robo4-UNC5B signaling maintains vascular integrity by counteracting VEGF signaling in endothelial cells, identifying a novel function of guidance receptor interactions in the vasculature.

INTRODUCTION

The vascular system is a highly branched network of arteries, capillaries, and veins that supplies all body tissues with oxygen and nutrients and removes waste. Endothelial cells (EC) that line mature blood vessels form a barrier that prevents leakage of protein and fluid into tissues. Formation of new blood vessels requires release of angiogenic growth factors such as VEGF, which disrupts the EC barrier and induces vascular leak and sprouting of new vessel branches (Adams and Alitalo, 2007; Gavard and Gutkind, 2006). Activation of quiescent EC by VEGF is mediated by binding to its high affinity receptor VEGFR2 and receptor autophosphorylation, which leads to activation of intracellular signaling cascades that execute VEGF signaling, including Src family kinases (Eliceiri et al., 1999; Gavard and Gutkind, 2006). Appropriate regulation of the VEGF response is required to ensure vessel stability, patterning of neovessels and proper tissue blood supply.

Recent studies have suggested that Robo4 inhibits VEGF downstream signaling (Jones et al., 2008, 2009; London et al., 2010; Marlow et al., 2010). Robo4 belongs to a family of four Roundabout receptors identified in vertebrates. Robo1-3 are single-pass transmembrane receptors for repulsive axon guidance molecules of the Slit family. Robo1-3 participate in the guidance of commissural axons by preventing axons that have crossed the midline from re-crossing (Brose et al., 1999; Dickson and Gilestro, 2006; Kidd et al., 1998; Long et al., 2004; Stein and Tessier-Lavigne, 2001). In contrast to the other Robo receptors, which are mainly expressed in the nervous system, Robo4 expression is selective for vascular EC, including the tumor vasculature (Huminiecki et al., 2002; Okada et al., 2007). *Robo4*$^{-/-}$ mice are viable, but exhibit increased basal and VEGF-induced retinal vascular permeability and show hypervascularization during experimentally induced pathological ocular neovascularization (Jones et al., 2008). These data suggest that Robo4 is required to maintain blood vessel integrity by counteracting VEGF and acts as a negative regulator of angiogenesis in these model systems.

Compared to the other Robo receptors, Robo4 is not only expressed in a different tissue environment (i.e., the vascular system as opposed to the nervous system), but is also structurally divergent and contains only two IgG-like domains and two FNIII repeats in the extracellular domain (ECD) and lacks the CC1 and CC3 motifs found in the intracellular domain of most other Robo proteins (Fukuhara et al., 2008; Hussain et al., 2006; Morlot et al., 2007). As the ECD is structurally divergent, it remains currently unclear if Robo4 can bind to Slit proteins. Binding of Slit-2 to Robo4 has been shown using supernatant from myc-tagged Slit-2 transfected cells added to Robo4

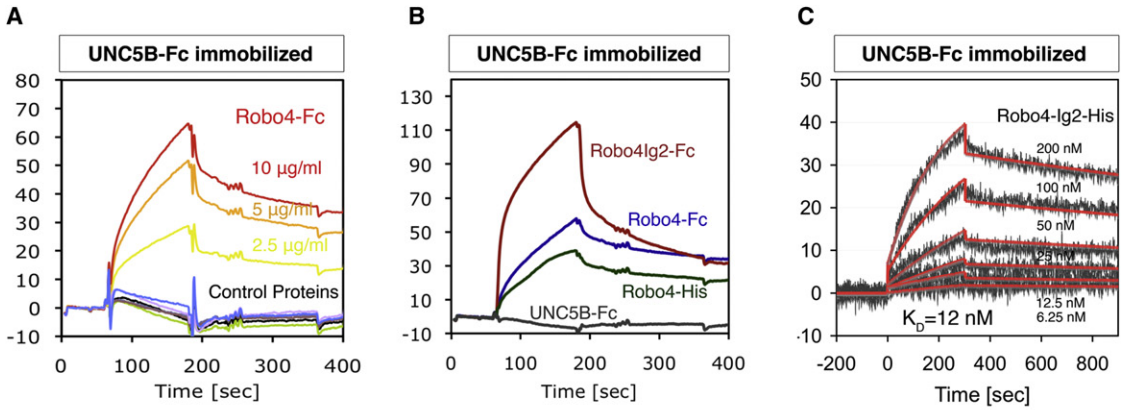
A
UNC5B-Fc immobilized
Robo4-Fc
10 μg/ml
5 μg/ml
2.5 μg/ml
Control Proteins
Time [sec]
B
UNC5B-Fc immobilized
Robo4Ig2-Fc
Robo4-Fc
Robo4-His
UNC5B-Fc
Time [sec]
C
UNC5B-Fc immobilized
Robo4-Ig2-His
200 nM
100 nM
50 nM
25 nM
12.5 nM
6.25 nM
K_D=12 nM
Time [sec]

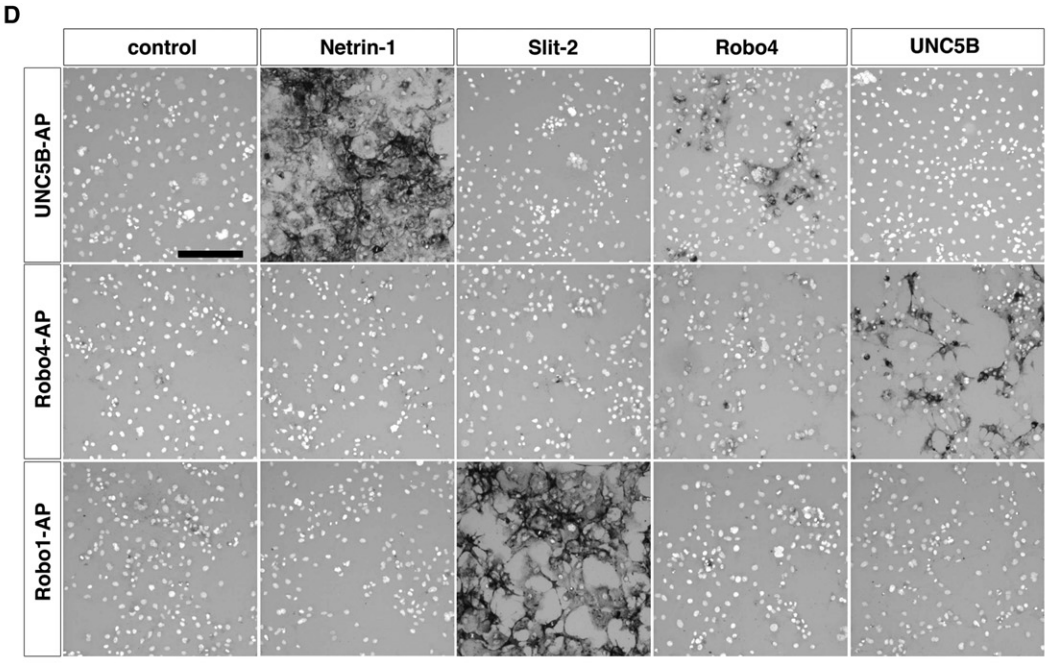
D
control
Netrin-1
Slit-2
Robo4
UNC5B
UNC5B-AP
Robo4-AP
Robo1-AP

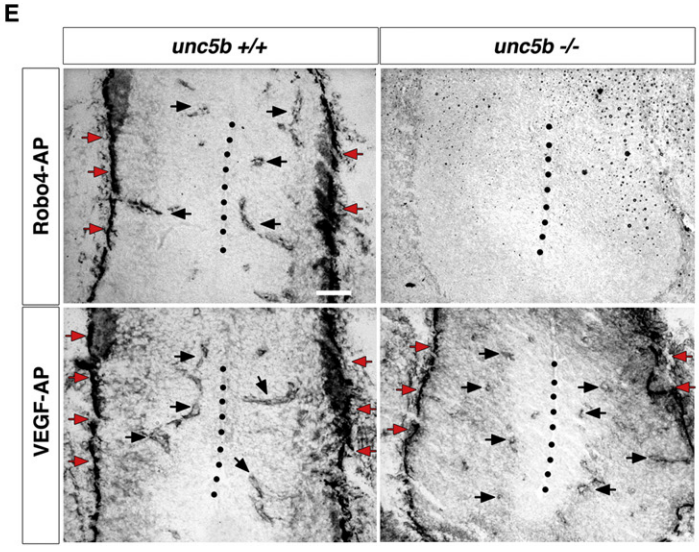
E
unc5b +/+
unc5b -/-
Robo4-AP
VEGF-AP

expressing cells or in ELISA assays (Park et al., 2003; Zhang et al., 2009), whereas Slit binding to Robo4 has not been observed in Biacore binding assays (Suchting et al., 2005). As Robo4 function seems critical for proper vascular patterning, we set out to identify molecules binding to the Robo4 extracellular domain. Using a protein-protein interaction screen with a Robo4 extracellular domain (ECD)-Fc fusion protein as a bait, we identified a single interaction partner, which surprisingly turned out to be another vascular-specific axon guidance receptor, UNC5B (Leonardo et al., 1997; Lu et al., 2004). Our data show that Robo4 acts as a membrane-bound UNC5B ligand and support a model where UNC5B acts as a signaling receptor that is required to maintain vessel integrity and barrier function by blocking VEGF-mediated downstream signaling.

RESULTS

Robo4 Binds UNC5B with High Affinity

To identify putative Robo4 ligands, we used Robo4-ECD-Fc protein to screen ~1900 secreted proteins and ECD protein constructs of a secreted protein library (Clark et al., 2003) by biolayer interferometry. This protein-protein interaction screen revealed a highly selective interaction between Robo4 and the ECD of UNC5B, a vascular-specific Netrin receptor (Leonardo et al., 1997; Lu et al., 2004) (see Figures S1A and S1B available online). Surface plasmon resonance (SPR) direct binding experiments confirmed specific, dose-dependent binding of Robo4-Fc to UNC5B-Fc but not to a number of unrelated control proteins (Figure 1A). Fc- and His-tagged versions of the Robo4 ECD containing only the first two immunoglobulin-like (Ig-like) domains were sufficient to bind UNC5B, localizing the binding site within these domains; a K_D of 12 nM was measured for this interaction (Figures 1B and 1C), which is in the same range as the binding of Netrin-1 to UNC5B (3.4 nM) (Leonardo et al., 1997).

To confirm the SPR results in a cell-based assay, we expressed full-length Robo4, UNC5B, and Netrin-1 constructs in COS cells and incubated them with alkaline-phosphatase (AP)-tagged UNC5B and Robo4 ECD proteins (Figure 1D). UNC5B AP bound to Netrin-1 and Robo4, but not to Netrin-4 (data not shown) or to itself, whereas Robo4 AP only bound to UNC5B expressing cells (Figure 1D). UNC5B AP staining was restricted to cells expressing Robo4 and vice versa as demonstrated by immunofluorescence of cells transiently transfected with Robo4 GFP- or UNC5B Cherry-tagged receptor constructs (Figure S1C).

As Robo4 had previously been reported to bind to Slit-2, we also tested binding of the Robo4 and Robo1 ECD to Slit-2. Robo4-AP did not bind to cells expressing Slit-2, whereas a Robo1-ECD-AP fusion protein did (Figure 1D). Likewise, Slit-2-AP bound to cells expressing Robo1, but not to cells expressing Robo4 (Figure S1D). Recombinant purified Robo1 ECD efficiently bound Slit-2 in SPR binding experiments, whereas the Robo4 ECD failed to show Slit-2 binding (Figure S1E). Finally, Slit-2-AP binding was similar on tissues of wild-type and *Robo4*$^{-/-}$ mice (Figure S1F), demonstrating that Robo4 is not required for Slit-2 binding in vivo.

To determine if Robo4 binds to UNC5B in vivo, we incubated sections of E11.5 mouse embryos with AP-tagged Robo4 and VEGF proteins. VEGF-AP labeled EC expressing VEGF receptors in sections of both wild-type and *Unc5b*$^{-/-}$ embryos. Robo4-AP stained EC in the hindbrain and perineural vascular plexus in wild-type embryos expressing UNC5B, but no Robo4-AP staining was observed on sections of *Unc5b*$^{-/-}$ embryos (Figure 1E); in fact we could not detect staining in any part of the *Unc5b*$^{-/-}$ embryos (data not shown), demonstrating that UNC5B expression is required for Robo4 binding in vivo. These data show that UNC5B is a high-affinity binding partner for Robo4.

We used SPR binding assays to test if Robo4 and Netrin-1 bind to the same, or to distinct domains of the UNC5B ECD. Netrin-1 and Robo4 bind noncompetitively to an UNC5B construct that comprises the entire UNC5B ECD (Figure S1G). Netrin-1, but not Robo4 binds to a construct encoding only the N-terminal Ig-like domains, indicating that Robo4 and Netrin-1 bind to distinct UNC5B domains (Figures S1G and S1H).

Robo4 Acts as an UNC5B Ligand

Both Robo4 and UNC5B are transmembrane receptors with a cytoplasmic domain that could mediate signaling (Huminiecki et al., 2002; Leonardo et al., 1997). In addition, both receptor proteins are coexpressed in EC, as shown by whole-mount immunostaining of dermal capillaries and diaphragm (Figure 2A; Figure S2A). These observations raise several possible scenarios for Robo4-UNC5B interactions UNC5B and Robo4 could act as coreceptors and signal in *cis*, or, alternatively, they could signal in *trans* between neighboring endothelial cells, either uni- or bidirectionally.

To test if UNC5B can activate Robo4 signaling, we used porcine aortic EC (PAECs) expressing GFP-tagged full-length Robo4. Incubation of these cells with UNC5B-Fc did not stimulate Robo4 internalization (Figure 2B). However, we observed only low Robo4 levels at the PAEC surface, whereas most receptor localized to intracellular vesicles (data not shown). Cytoplasmic Robo4 localization was not affected by

Figure 1. Robo4 Binds UNC5B

(A–C) SPR binding measurements confirm that Robo4-Fc binds specifically to UNC5B. (A) UNC5B-Fc was immobilized onto a Biacore CM5 sensor chip and Robo4-Fc and six unrelated control proteins were injected at different concentrations for 120 s and allowed to dissociate for 240 s. (B) Different Robo4 constructs including Robo4-Ig2-Fc bind to immobilized UNC5B-Fc but UNC5B does not bind to itself (no homo association). (C) For affinity measurements UNC5B-Fc was immobilized onto a GLC chip (ProteOn, BioRad) and binding sensorgrams for six different Robo4-Ig2-His concentrations (6.25 to 200 nM) were recorded simultaneously. The equilibrium dissociation constant (K_D) was calculated from the on- and off-rates obtained by simultaneous fitting of the association and dissociation sensorgrams.

(D) COS cells transfected as indicated or untransfected (control) were seeded on triplicate wells and incubated with the indicated AP-fusion proteins. Representative images from one of three independent experiments are shown. UNC5B-AP binds Netrin-1 and Robo4, Robo4-AP binds UNC5B, and Robo1-AP binds Slit-2.

(E) AP-fusion protein binding to cryo sections from E11.5 hindbrains of *Unc5b*$^{+/+}$ or $^{-/-}$ embryos as indicated. Note absence of Robo4AP binding to *Unc5b*$^{-/-}$ EC. Dotted line: midline. Red arrows: perineural vascular plexus. Black arrows: intracerebral capillaries. Scale bars represent 50 μm (see also Figure S1).

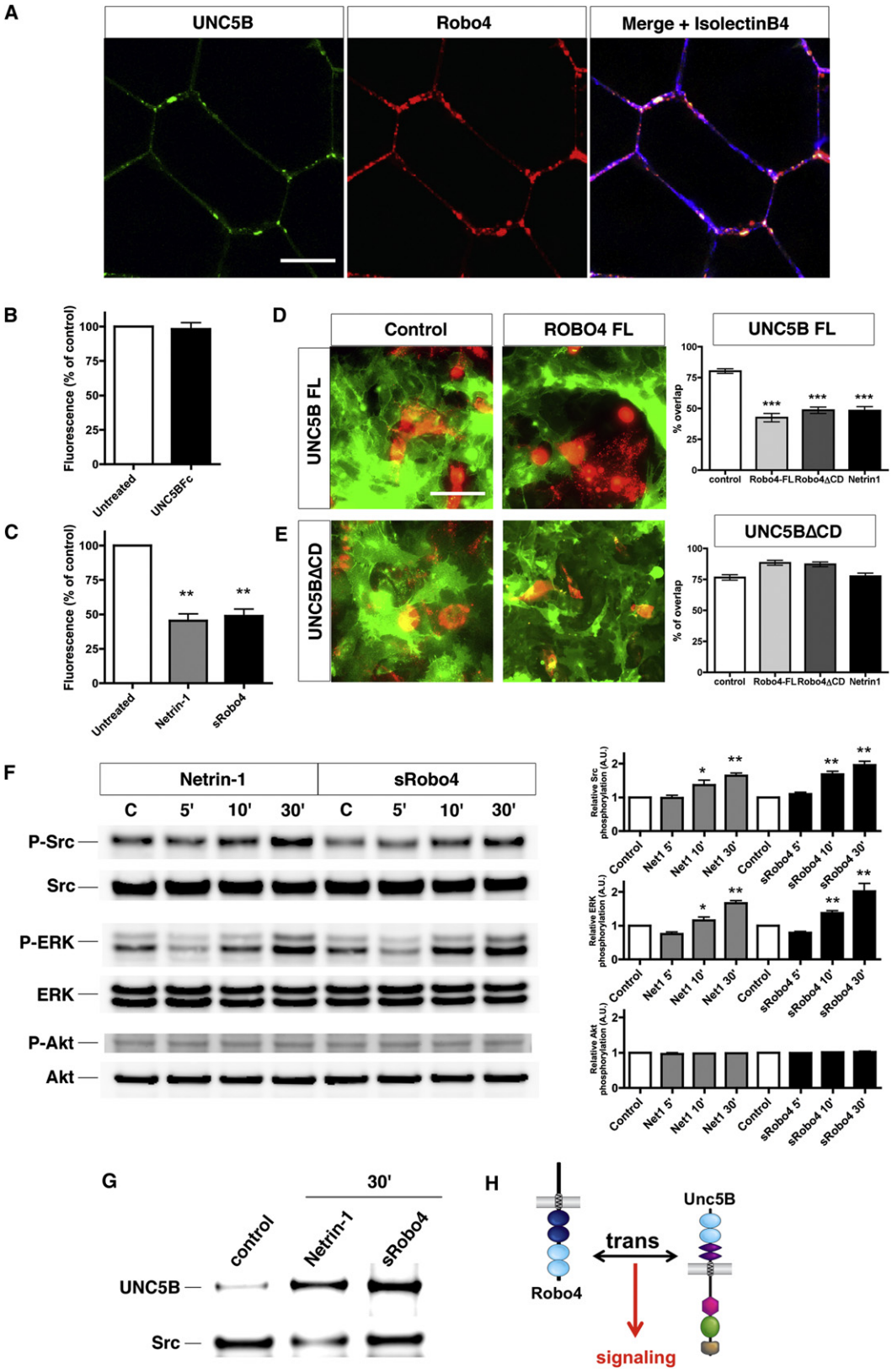
A
UNC5B
Robo4
Merge + IsolectinB4
B
Fluorescence (% of control)
Untreated
UNC5BFc
C
Fluorescence (% of control)
Untreated
Netrin-1
sRobo4
D
Control
ROBO4 FL
UNC5B FL
% overlap
control
Robo4-FL
Robo4ΔCD
Netrin1
E
UNC5BΔCD
UNC5BΔCD
% of overlap
F
Netrin-1
sRobo4
C
5'
10'
30'
P-Src
Src
P-ERK
ERK
P-Akt
Akt
Relative Src phosphorylation (A.U.)
Relative ERK phosphorylation (A.U.)
Relative Akt phosphorylation (A.U.)
Control
Net1 5'
Net1 10'
Net1 30'
sRobo4 5'
sRobo4 10'
sRobo4 30'
G
30'
control
Netrin-1
sRobo4
UNC5B
Src
H
Robo4
trans
Unc5B
signaling

coexpression of UNC5B within the same cell in *cis* or by stimulation with UNC5B in *trans* (data not shown). Radioligand cell binding experiments with a specific anti-Robo4 antibody (see below) revealed low cell surface copy numbers for endogenous Robo4 on murine (MS1) and human (HUVEC) ECs confirming the low Robo4 surface expression (Figures S2B and S2C). These results precluded further examination of possible Robo4 signaling effects after stimulation with UNC5B.

In contrast, stimulation of PAECs transfected with a GFP-tagged UNC5B-full-length construct (UNC5B-Fl) with Robo4-Ig2-His protein (hereafter termed sRobo4) or Netrin-1 led to UNC5B internalization and decrease of surface GFP fluorescence (Figure 2C; Figure S2D). To test activity of full-length Robo4, we cocultured UNC5B cells and 293 cells transfected with a Cherry-tagged Robo4-Fl construct. Video-microscopy showed that as soon as a Robo4 expressing cells touched an UNC5B-Fl expressing cells, GFP-tagged UNC5b receptors aggregated and the cells retracted from the Robo4 expressing cells (data not shown). Repulsion was quantified after 24 hr of coculture, by measuring the overlap between red 293 cells and green UNC5B PAECs. In control cocultures between untransfected red labeled 293 cells and UNC5B-Fl PAECs, cells mix, leading to overlap of red cells by green cells, with ~80% of the surface area of the control 293 cells covered by PAECs (Figure 2D). Repulsion of UNC5B cells by Robo4-Fl cells leads to segregation of the two populations, i.e., significant reduction in overlap of red and green cells compared to controls (Figure 2D). Expression of a truncated Robo4 receptor lacking the cytoplasmic signaling domain (Robo4ΔCD) in 293 cells was sufficient to repel UNC5B-expressing PAECs (Figure 2D). Coculture with 293 cells expressing Netrin-1 likewise induces UNC5B repulsion and segregation (Larrivee et al., 2007) (Figure 2D).

Expression of a truncated UNC5B receptor lacking the cytoplasmic signaling domain (UNC5BΔCD) in PAECs abolished retraction in response to 293 cells expressing Robo4-Fl, Robo4ΔCD, and Netrin-1, indicating that UNC5B signaling is required for repulsion to occur (Figure 2E). Robo4 therefore acts as a repulsive transmembrane ligand for UNC5B when presented in *trans*, similar to the established secreted ligand Netrin-1.

To examine if Robo4 triggered signaling events in EC expressing endogenous UNC5B, serum-starved human umbilical artery EC (HUAECs) were incubated with Netrin-1 and sRobo4. Both ligands increased phosphorylation levels of ERK and Src, but did not stimulate AKT phosphorylation (Figure 2F). Stimulation of EC isolated from *Unc5b*$^{-/-}$ mice with sRobo4 failed to increase Src phosphorylation, indicating that UNC5B is required for Src activation in response to sRobo4 (Figure S2E). Immunoprecipitation with an anti-Src antibody and western blotting with anti-UNC5B showed that UNC5B coimmunoprecipitated with Src after stimulation with Netrin-1 or sRobo4 (Figure 2G). To test if blocking Src phosphorylation inhibited UNC5B signaling and biological response, we cocultured Robo4 expressing 293 cells with UNC5B expressing PAECs in the presence or absence of the Src family kinase inhibitor PP2 (Hanke et al., 1996). PP2 treatment efficiently blocked Src phosphorylation in PAECs and did not alter PAEC morphology or cell division (data not shown). However, PP2 completely blocked segregation of UNC5B expressing PAECs from Robo4 expressing 293 cells (Figure S2F). These results support a model in which Src activation and association with UNC5B is required for signal transduction and response to Robo4 (Figure 2H).

Generation of Antibodies Blocking Robo4 and UNC5B

To explore biological effects of Robo4-UNC5B interactions, we generated high-affinity, phage-derived monoclonal antibodies (mAbs) against the N-terminal Robo4 IgG like domains (Figure 3A). Among several candidates, we identified one antibody, anti-Robo4-1, that efficiently blocked binding of Robo4 to UNC5B-Fc in SPR binding assays, whereas two other antibodies, anti-Robo4-2 and anti-Robo4-3 only partially blocked UNC5B binding (Figure 3B). Based on these SPR data, anti-Robo4-1 was used in all subsequent experiments. Anti-Robo4-1 is an affinity matured, phage-derived human IgG1 mAb that binds with a K_D of 1 nM to human and murine Robo4 in SPR and in cell binding (HUVECs, MS1) experiments (N.R., unpublished data). Treatment of UNC5B-GFP PAECs with anti-Robo4-1 blocked sRobo4-induced UNC5B internalization (Figure 3C). In cocultures between UNC5B-GFP PAECs and Robo4-Cherry-expressing 293 cells, anti-Robo4-1 blocked Robo4- induced cell segregation (Figure S3A). These data show that anti-Robo4-1 efficiently blocks Robo4-UNC5B interactions in solution and in cells.

Figure 2. Robo4 Acts as an UNC5B Ligand

(A) Confocal images of dermal capillaries from 6-week-old wild-type mice labeled with anti-UNC5B (R&D), anti-Robo-4-1 and IsolectinB4. Note coexpression of Robo4 and UNC5B in EC.

(B) PAECs expressing GFP-tagged Robo4 were incubated with UNC5B-Fc and analyzed by FACS. Histograms of fluorescence intensity compared to untreated cells are shown. Note no change in surface fluorescence after treatment.

(C) PAECs expressing GFP-tagged UNC5B were incubated with Netrin-1 and Robo4-Ig2-His (sRobo4) and analyzed by FACS. Note decrease in surface fluorescence after ligand treatment.

(D) Robo4 repels UNC5B expressing cells when presented in *trans*. UNC5B-Fl expressing PAECs were cocultured with red-labeled untransfected (control) or transfected 293 cells as indicated. Cell mixing in control cocultures leads to overlap of red cells by green cells, which was measured on 10 images/well in three independent experiments. Expression of Robo4-Fl, Robo4ΔCD, or Netrin-1 in 293 cells induces repulsion of UNC5B cells, which leads to a reduction in overlap of red cells by green cells.

(E) Expression of UNC5BΔCD in PAECs abolishes repulsion.

(F) HUAECs were serum starved (control) and stimulated with Netrin-1 or sRobo4 as indicated. Protein extracts were subjected to sodium dodecyl sulfate polyacrylamide gel electrophoresis and western blots were incubated with the indicated antibodies. Both Netrin-1 and sRobo4 stimulate Src and ERK phosphorylation.

(G) PAECs expressing UNC5B were serum starved (control) and stimulated with ligands for 30 min, followed by Src immunoprecipitation and western blotting with an anti-UNC5B antibody (R&D). Both UNC5B ligands enhance UNC5B association with Src.

(H) Robo4 activates UNC5B signaling. Scale bars: 15 μm (A), 30 μm (D and E). Error bars represent standard error of the mean (SEM). $^{**}p < 0.01$, $^{***}p < 0.001$ (Student's t test) (see also Figure S2).

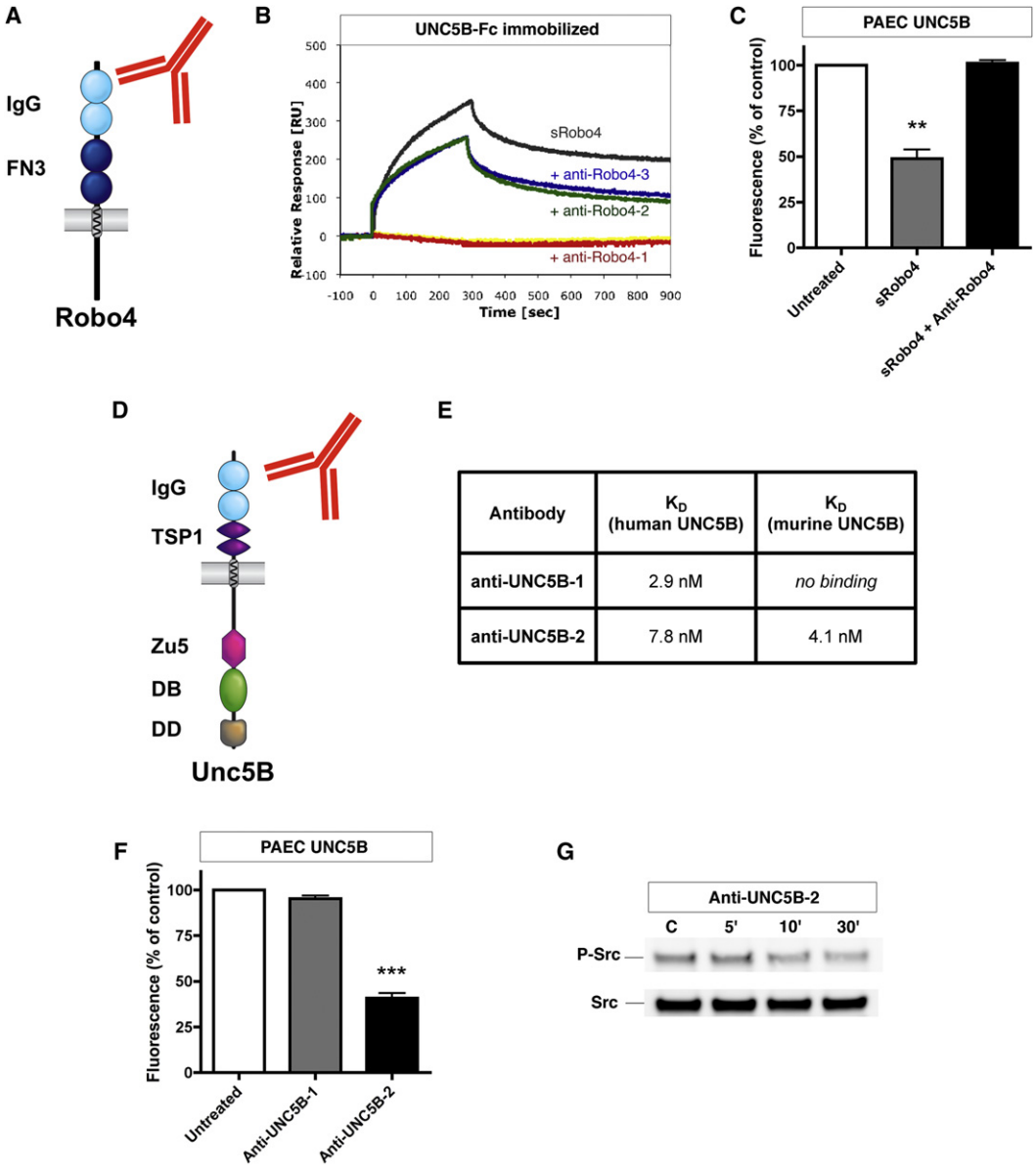

Antibody	K_D (human UNC5B)	K_D (murine UNC5B)
anti-UNC5B-1	2.9 nM	*no binding*
anti-UNC5B-2	7.8 nM	4.1 nM

Figure 3. Generation of Function Blocking Anti-Robo4 and Anti-UNC5B Antibodies

(A) Schematic diagram of Robo4. Phage derived antibodies were raised against the two N-terminal Ig domains of Robo4.

(B) Anti-Robo4-1 blocks Robo4 binding to UNC5B. For SPR binding and binding/competition experiments UNC5B-Fc was immobilized onto a ProteOn GLC sensor chip and sRobo4 or equimolar mixtures of sRobo4 with anti-Robo4 antibodies were injected and allowed to bind for 240 s. Note that the decrease of the binding signal for the Robo4/anti-Robo4-2 and -3 complexes indicates that these antibodies interfere with the Robo4-UNC5B interactions whereas a complete loss of binding for the Robo4/anti-Robo4-1 complex shows that Robo4-1 completely blocks the interaction.

(C) Pretreatment of UNC5B-GFP expressing PAECs with anti-Robo4-1 (50 μg/ml) blocks sRobo4 induced UNC5B internalization.

(D) Schematic diagram of UNC5B. Phage derived antibodies were raised against the two N-terminal Ig domains of UNC5B.

(E) Binding affinities for anti-UNC5B antibodies to human and murine UNC5B as determined by SPR measurements.

(F) UNC5B-GFP expressing PAECs were cultured in the presence of 100 μg/ml anti-UNC5B-1 or anti-UNC5B-2 for 12 hr. FACS analysis shows that anti-UNC5B-2, but not anti-UNC5B-1, causes UNC5B internalization and decrease of surface GFP fluorescence.

(G) Analysis of Src and phospho-Src levels in HUAECs treated with anti-UNC5B-2. Error bars represent SEM. $^{**}p < 0.01$, $^{***}p < 0.001$ (Student's t test) (see also Figure S3).

We also generated phage-derived mAbs directed against the IgG-like domains of human UNC5B (Figure 3D). One antibody, anti-UNC5B-1, bound human but not mouse UNC5B, whereas anti-UNC5B-2 bound both human and mouse receptors with high affinity (Figure 3E). SPR experiments showed that anti-UNC5B-2 interferes with Netrin-1 binding to immobilized UNC5B-Fc (Figure S3B). Incubation of UNC5B-GFP PAECs with anti-UNC5B-2, but not with anti-UNC5B-1, induced

UNC5B internalization (Figure 3F). In vivo injection of anti-UNC5B-2 (20 mg/kg, P0 and P3) into neonatal mice followed by staining of the retinal vasculature with a polyclonal anti-UNC5B antibody at P5 also led to almost total disappearance of UNC5B labeling in the vasculature (Figure S3C). Anti-UNC5B-2 did not induce Src phosphorylation in HUAECs (Figure 3G), indicating that anti-UNC5B-2 does not activate UNC5B signaling, but blocks UNC5B function by inducing internalization.

Robo4 UNC5B Signaling Counteracts VEGF-Mediated Src Activation

As Robo4 stimulation of HUAECs recruited phospho-Src to UNC5B, we hypothesized that this could reduce phospho-Src association with VEGFR2 and so reduce VEGFR2 activity. We stimulated HUAECs or primary wild-type mouse EC with VEGF in the presence of anti-Robo4-1 or anti-UNC5B-2 antibodies to block the Robo4-UNC5B interaction, or of sRobo4 to activate UNC5B (Figures 4A and 4B). After VEGFR2 immunoprecipitation, anti-UNC5B-2 and anti-Robo4-1 significantly increased VEGF-mediated Src and phospho-Src association to VEGFR2 (Figures 4A and 4B). Conversely, stimulation of UNC5B with sRobo4 decreased VEGF-mediated Src and phospho-Src association to VEGFR2 (Figures 4A and 4B). VEGF-treated *Unc5b*$^{-/-}$ mouse EC did not show any detectable changes in Src association with VEGFR2 after sRobo4 or blocking antibody treatment (Figure 4C), supporting a model whereby Robo4 activation of UNC5B competes with VEGF-VEGFR for Src activation and downstream signaling by sequestering Src away from VEGFR2.

Blocking Robo4-UNC5B Interaction Increases Angiogenesis In Vivo

Because Robo4-UNC5B counteracts VEGF signaling in vitro, we exploited the mouse corneal pocket assay to test if the Robo4-UNC5B interaction has an effect on VEGF-mediated angiogenic sprouting. Intraperitoneal injection with anti-Robo4-1 significantly increased corneal neovascularization (Figures 4D and 4E) similar to the increase seen in *Robo4*$^{-/-}$ mice compared to wild-type littermates (N.R., unpublished data). Treatment with anti-UNC5B-2 also induced significant corneal hypervascularization (Figures 4D and 4E). Compared to anti-Robo4-1 treatment, anti-UNCB-2 treatment leads to a different phenotype in the cornea, i.e., smaller total neovessel area, but denser more disorganized vessels at the leading front (Figure 4E; Figure S4). These observations suggest that Robo4 could act independently of UNC5B during corneal neovascularization. We therefore treated animals with anti-Robo4-1 and anti-UNC5B-2 simultaneously. The hypervascularization of this combination treatment quantitatively and qualitatively mimics the anti-UNC5B-2 treatment (Figures 4D and 4E), supporting our cell-based data that Robo4 and UNC5B interact and that Robo4 acts upstream of UNC5B.

Robo4 Is Dispensable for Developmental Angiogenesis

To investigate if blocking UNC5B-Robo4 interactions has an effect on developmental angiogenesis we treated neonatal mice with function-blocking antibodies. Treatment with anti-UNC5B-2 caused significant hypervascularization of retinal vessels, mimicking the effect of genetic loss of *Unc5b* function (Figure 5). In contrast, anti-Robo4-1 treated or *Robo4*$^{-/-}$ mice showed normal retinal vascular development (Figure 5). UNC5B is therefore required in the developing vasculature to prevent excessive branching, confirming and extending previous results (Bouvree et al., 2008; Larrivee et al., 2007; Lu et al., 2004). Robo4 function in the developing vasculature is dispensable; suggesting that absence of Robo4 may be compensated by another UNC5B ligand.

Blocking Robo4 UNC5B Interaction Causes Vessel Hyperpermeability

As *Robo4*$^{-/-}$ mice exhibit increased basal retinal vascular permeability (Jones et al., 2008), we tested if this was due to disruption of Robo4-UNC5B interactions. We injected fluorescent microspheres into *Robo4*$^{-/-}$ mice and mice treated with blocking mAbs. Microsphere extravasation was significantly enhanced in *Robo4*$^{-/-}$ mice and mice treated with anti-Robo4-1 and anti-UNC5B-2 compared to mice injected with anti-UNC5B-1 control mAb (Figure 6A). This indicates that blocking Robo4-UNC5B interaction disrupts retinal vessel barrier integrity. To quantify vessel barrier function, we used a Miles assay, where Evan's blue is injected into the tail vein, followed by intradermal injection of VEGF or saline and quantification of dye leak into the skin. *Robo4*$^{-/-}$ mice exhibited significant increase in basal endothelial permeability compared to wild-type littermates (Figure 6B). The breakdown of endothelial barrier function seen in *Robo4*$^{-/-}$ mice could be mimicked by intradermal injection of anti-UNC5B-2 and anti-Robo4-1 (Figure 6C).

Increased basal vascular permeability in *Robo4*$^{-/-}$ mice and mice treated with the blocking antibodies was expected to activate compensatory physiological responses to maintain blood pressure. *Robo4*$^{-/-}$ mice and mice treated with anti-UNC5B-2 or anti-Robo-4-1 for four days showed a significant increase in plasma renin levels and in the number of renin^{+} glomeruli compared to wild-type mice or mice treated with anti-UNC5B-1 (Figures S5A and S5B). Activation of the renin-angiotensin system therefore contributes to physiological adaptation to vessel barrier breakdown after disruption of the Robo4-UNC5B interaction.

If Robo4 maintains vessel integrity by activating UNC5B, soluble Robo4 protein should rescue vessel hyperpermeability in *Robo4*$^{-/-}$ mice. Indeed, intradermal injection of sRobo4 into *Robo4*$^{-/-}$ mice restored vessel barrier function (Figure 6B). SRobo4 also reduced VEGF-induced hyperpermeability in wild-type mice, but not in mice treated with anti-UNC5B-2 (Figures 6D and 6E), supporting a model whereby Robo4 maintains vessel integrity by binding and signaling through UNC5B. Because blocking of the Robo4-UNC5B interaction increased Src association with VEGFR2 in vitro (Figures 4A and 4B), we reasoned that vessel barrier breakdown might reflect excessive VEGF signaling and Src kinase activation. Accordingly, combined treatment using anti-UNC5B-2 or anti-Robo4-1 together with s-flt-1 or PP2 restored vessel barrier function (Figures 6F and 6G).

Vascular permeability is known to be regulated in part by Src, which phosphorylates VE-cadherin and promotes its internalization and disassembly of intercellular junctions. To test if Robo4-UNC5B interactions would influence VE-cadherin phosphorylation, we treated HUAECs with VEGF in the presence of sRobo4,

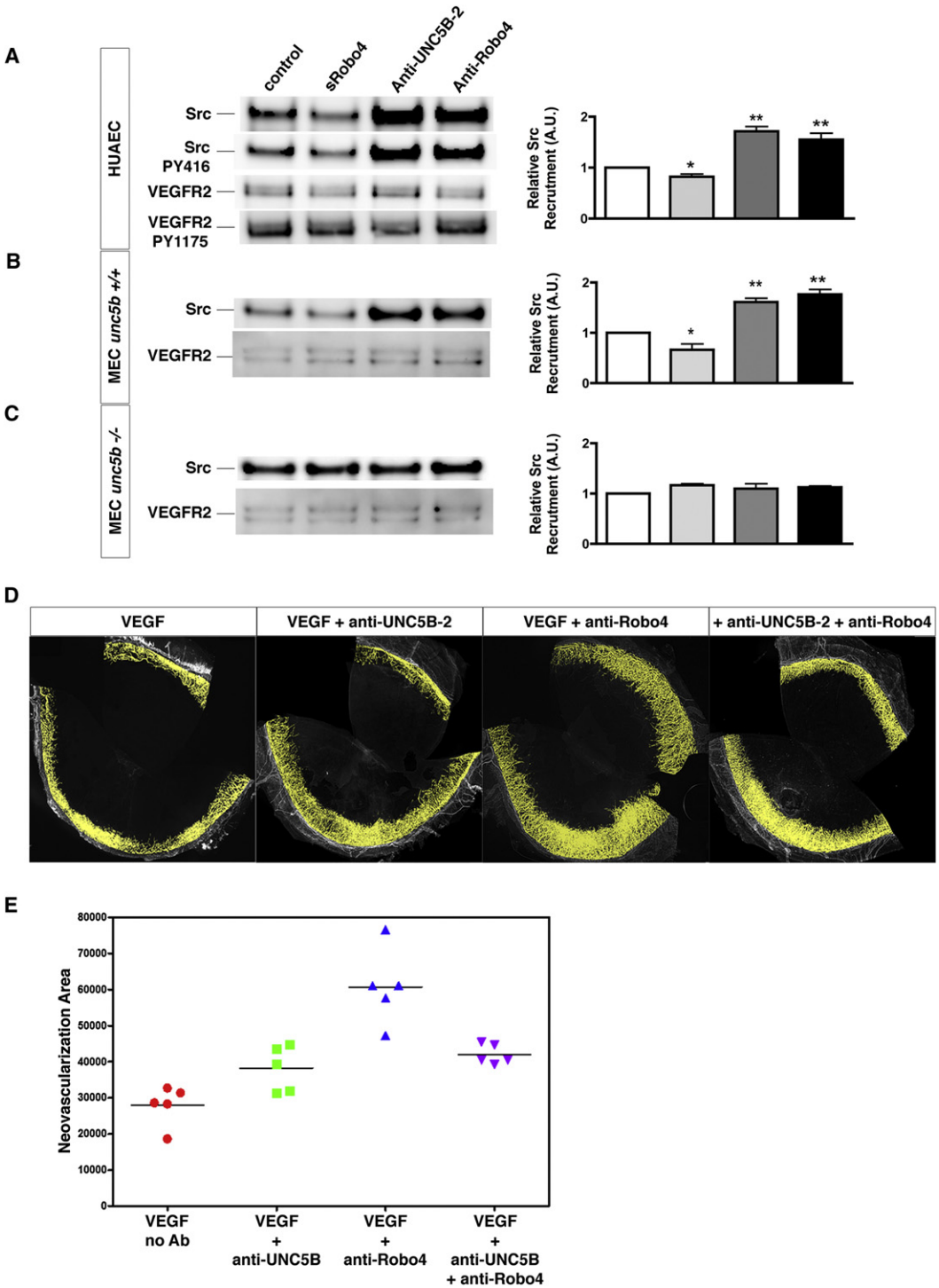

Figure 4. Robo4-UNC5B Counteracts VEGF Signaling In Vitro and VEGF-Induced Neovascularization In Vivo

(A) HUAECs, (B) wild-type, and (C) *Unc5b*$^{-/-}$ mouse ECs were serum starved and stimulated with VEGF for 5 min. Parallel cultures were pre-treated with sRobo4, anti-Robo4-1, or anti-UNC5B-2 before VEGF stimulation. VEGFR2 was immunoprecipitated from cultures and western blots were probed with indicated antibodies. Pretreatment with sRobo4 decreases Src and phospho-Src association with VEGFR2, while blocking of the Robo4-UNC5B interaction with anti-UNC5B-2 or anti-Robo4-1 increases Src association with VEGFR2 compared to control in (A) and (B), but not in *Unc5b*$^{-/-}$ EC (C). VEGFR2 and phospho-VEGFR2 levels are similar in all treatment conditions. Quantification of four independent experiments is shown. Bars represent SEM. *$p < 0.05$, **$p < 0.01$ (Mann-Whitney test).

(D and E) Mouse corneal pocket assay (D) Representative images of entire corneas stained with anti-CD31 illustrating the effects of intracorneal placement of a 175 ng pellet of VEGF and systemic treatment (i.p. injection) of anti-Robo4-1 (20 mg/kg), anti-UNC5B-2 (25 mg/kg), and combined treatment with both antibodies. (E) Quantification of the neovascularization area from the experiment described in (D). All groups are statistically significantly different from each other, except for anti-UNC5B-2 and anti-UNC5B-2 + anti-Robo4-1 treatment groups (see also Figure S4).

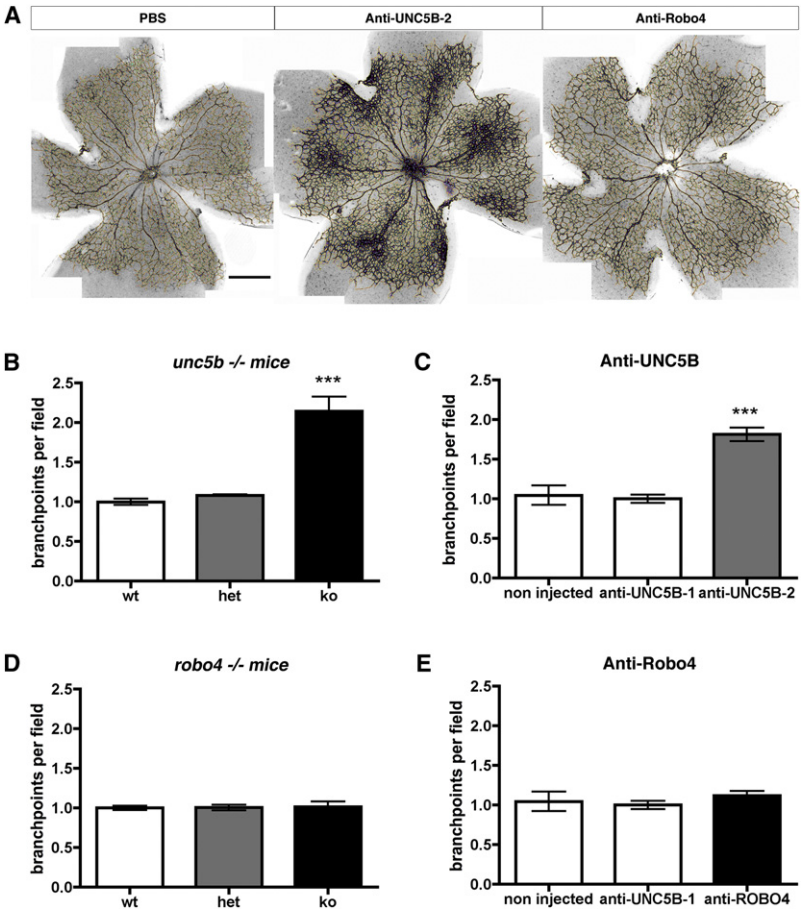

Figure 5. Blocking UNC5B, But Not Robo4, Leads to Retinal Hypervascularization

(A) Confocal images of isolectin-B4 stained retinal whole-mounts at P5 after IP treatment with the indicated antibodies (25 mg/ml) at P1, P2, P3, and P4. The number of branch points per retina was quantified using computer-assisted software (see yellow and blue pixels on the images after zooming in). Scale bar represents 125 μm.

(B) Quantification of retinal vascularization in P5 CD1-*Unc5b-LacZ-plap* mice. Wild-type values were set as 1 (corresponding to a total of 5478 ± 355 branch points per retina). Note hypervascularization in *Unc5b*$^{-/-}$ retinas (corresponding to 10639 ± 1258 branch points per retina). Seven litters comprising viable *Unc5b*$^{-/-}$ pups with weight comparable to wild-type littermates were analyzed. (WT, n = 12; het, n = 14; KO, n = 12).

(C) Quantification of retinal vascularization after anti-UNC5B treatment. C57/Bl6 litters (n = 4) were injected and values in noninjected wild-type littermates were set as 1 in (C) and (E). (noninjected, n = 6; anti-UNC5B-1, n = 13; anti-UNC5B-2, n = 17). Note that anti-UNC5B-1, which does not bind to mouse UNC5B has no effect on retinal vascular development, whereas anti-UNC5B-2 leads to hypervascularization.

(D) Quantification of retinal vascularization in P5 *Robo4* mice. Wild-type values were set as 1 (corresponding to a total of 4834 ± 239 branch points per retina on a C57/Bl6 background). Four litters were analyzed. (WT, n = 5; het, n = 8; KO, n = 8).

(E) Quantification of retinal vascularization after anti-Robo4-1 treatment. Three litters were analyzed. (non-injected, n = 6; anti-UNC5B-1, n = 13; anti-ROBO4, n = 10). Note no change in retinal vascularization in *Robo4*$^{-/-}$ (D) or after anti-Robo4-1 treatment (E). ***$p < 0.001$, Mann-Whitney test.

anti-Robo4-1, or anti-UNC5B-2. SRobo4 decreased VE-cadherin phosphorylation, whereas anti-UNC5B-2 and anti-Robo4-1 significantly increased VEGF-mediated VE-cadherin phosphorylation (Figure S5C). Therefore, phospho-Src and VEGF-stimulated phospho-VE-cadherin both respond to activation or inhibition of the Robo4-UNC5B pathway, supporting a model where Robo4 activation of UNC5B competes with VEGF for downstream Src activation, VE-cadherin phosphorylation, and junctional disassembly (Figure 7).

DISCUSSION

Robo4 Binds UNC5B

The results presented here identify UNC5B as a Robo4 binding partner. We show that the Robo4 ECD selectively binds to the UNC5B ECD in a large-scale protein interaction screen. SPR binding assays confirm specific Robo4-UNC5B binding and show that the N-terminal 2 Ig-like domains of Robo4 are sufficient to bind to the thrombospondin-like domains of UNC5B with high affinity. In cell-based binding assays, Robo4 and UNC5B selectively bind to each other, and the presence of UNC5B in vivo is required for Robo4-AP binding. Although we cannot exclude that additional, as yet unidentified Robo4 ligands exist, UNC5B may be the major Robo4 partner in vivo, because Robo4 binding was completely abolished in *Unc5b* deficient embryos, and because among ~1900 protein samples, comprising ~1000 individual proteins, only UNC5B-Fc bound Robo4.

Absence of Robo4-Slit-2 Binding

Our data fail to provide any evidence for Slit-2 binding to Robo4, arguing against Robo4 as a Slit-2 receptor, as reported previously (Hohenester et al., 2006; Suchting et al., 2005). In further support of the idea that Robo4 is not a receptor for Slits, a recent high resolution structure of the two N-terminal Ig like domains of Robo1 identified key Slit binding residues and revealed a heparan sulfate/heparin binding site that strengthens the Slit-Robo1 interaction (Fukuhara et al., 2008; Hussain et al., 2006; Morlot et al., 2007). Although the N-terminal Ig like domains of Robo1 and Robo4 are 42% identical, none of the residues identified as Slit or heparin binding are conserved in Robo4, and they are replaced by residues that appear incompatible with binding Slits or heparin. Consistent with their structural analysis of Slit-Robo1 binding, Fukuhara et al. (2008) also reported that Robo4 did not bind to a heparin affinity column. In contrast to these data, another group has reported that Slit-2 functions via Robo4 to inhibit VEGF downstream responses, preventing excessive angiogenesis and permeability (Jones et al., 2008; London et al., 2010; Marlow et al., 2010; Park et al., 2003). Treatment of mice with Slit-2 was shown to decrease vascular permeability and angiogenesis in response to VEGF and inflammatory stimuli,

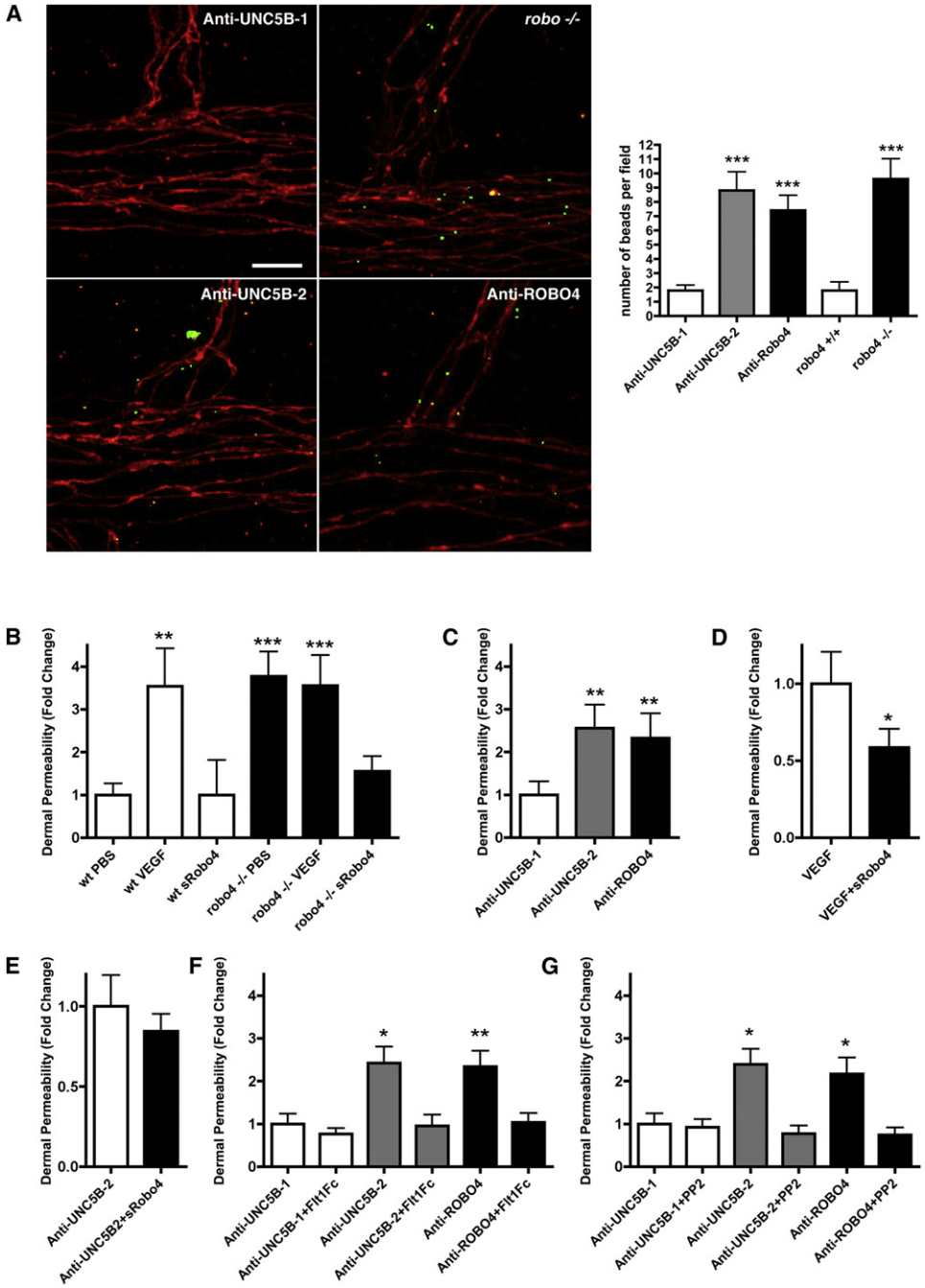

Figure 6. Robo4-UNC5B Interactions Stabilize Vessels

(A) Confocal images of fluorescent microsphere extravasation (green) from VE-cadherin-stained retinal vessels (red) of mice as indicated. Scale bar represents 10 μm. Quantification of bead extravasation on 10 images/retina from 3 animals/group is shown.

(B–G) A Miles assay was used to measure dermal microvessel permeability. Each panel corresponds to 4–10 mice per group. Bars represent SEM. $^{**}p < 0.01$ (Mann-Whitney test). (B) Increased basal vessel permeability in *Robo4*$^{-/-}$ mice is rescued by intradermal injection of 2ug sRobo4. (C) Intradermal injection of 20 μg anti-Robo4-1 and UNC5B-2 increases vessel permeability. (D) sRobo4 reduced hyperpermeability induced by VEGF (50 ng) in wild-type mice. (E) sRobo4 does not decrease vessel permeability in mice treated with anti-UNC5B-2. (F and G) Increased vessel permeability induced by antibody treatment is rescued by injection of sflt-1 (2 μg) (F) or PP2 (10 μM) (G). Bars represent SEM. $^{*}p < 0.05$, $^{***}p < 0.001$ (Mann-Whitney test) (see also Figure S5).

thus providing a protective endothelial barrier capable of rendering mice resistant to bacterial infections (Jones et al., 2008; London et al., 2010). Slit-2 responses were lost in *Robo4*-deficient mice, indicating that Slit-2 acted in a Robo4-dependant manner. However, Slit-2 might bind EC via other receptors, including Robo1 or Syndecans (London et al., 2010). Robo4

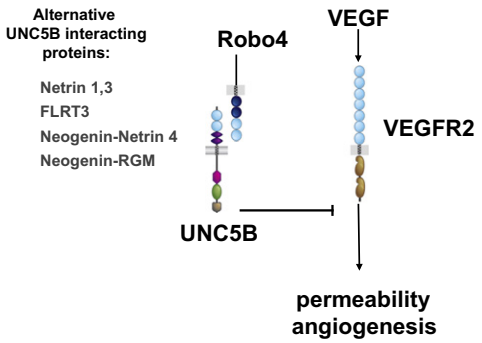

Figure 7. Working Model for Robo4-UNC5B Interaction

The data suggest that Robo4 inhibits VEGF-driven permeability and angiogenesis by binding and signaling through UNC5B, likely by activating UNC5B on neighboring cells in *trans*. Blocking Robo4-UNC5B interaction enhances VEGF-driven permeability and angiogenesis in vivo, indicating that Robo4-UNC5B signaling counteracts VEGF signaling. Absence of Robo4, e.g., in the developing vasculature, can be compensated for by alternative UNC5B interacting proteins, including several possible candidates, i.e., Netrin-1, Netrin-3, FLRT3, or Netrin-4 and RGM via Neogenin.

can be coimmunoprecipitated with Robo1 in cultured EC in vitro (Kaur et al., 2008; Sheldon et al., 2009), suggesting that Robo1-Robo4 heterodimerization could confer Slit responsiveness, leading to Robo1 and/or Robo4 signaling and cellular responses (Huminiecki et al., 2002; Kaur et al., 2008; Tang et al., 2008). Our data do not exclude such a scenario, however, we did not detect Robo1-Robo4 interactions by SPR in vitro, nor could we detect any Robo1 expression in EC in vivo, using in situ hybridization on mouse embryos (data not shown). Clearly, additional work is required to understand Slit-2 actions during angiogenesis in vivo.

Robo4 Activates UNC5B Signaling and Inhibits VEGF-Mediated VEGFR2 Signaling

Previous studies have shown that Robo4 can associate with intracellular signaling molecules including WASP, cdc42, and Rac1, indicating potential signaling roles of Robo4 (Kaur et al., 2008; Sheldon et al., 2009). Our results do not exclude such a possibility, although we have no evidence for Robo4 signaling. Stimulation of Robo4-expressing PAECs with UNC5B failed to elicit Robo4 internalization. Moreover, we consistently observe low Robo4 cell surface expression in primary cultured EC and on transfection of Robo4 constructs. Rather than acting as a receptor, our data support a model where Robo4 functions as a ligand for the UNC5B receptor in the vasculature (Figure 7). Robo4 activates UNC5B, Src phosphorylation and Src association with UNC5B, which decreases Src kinase association with VEGFR2 and VE-cadherin phosphorylation after VEGF stimulation. Conversely, blocking Robo4-UNC5B interaction and UNC5B signaling increases Src kinase association with VEGFR2 and VE-cadherin phosphorylation, suggesting that Robo4-UNC5B competes with VEGF-VEGFR2 for downstream signaling cascades in EC.

Robo4-UNC5B Interactions Inhibit Angiogenesis in a Corneal Pocket Assay, but Not during Development

Using corneal pocket assays with VEGF-containing implants, we show that treatment with anti-Robo4 and anti-UNC5B antibodies causes hypervascularization in response to VEGF, similar to the phenotype seen in *Robo4*$^{-/-}$ mice. Thus, both Robo4 and UNC5B appear to negatively regulate angiogenesis in this in vivo model. However, vessel morphologies are different between groups: anti-Robo4 treated corneas exhibit less-branched mostly vertical vessels, whereas anti-UNC5B treatment leads to more highly branched vessels with horizontal sprouting, resulting in generally denser vessels at the leading front (Figure S4). In addition to these morphological differences, the neovascularization area induced by anti-Robo4 treatment is also larger than the one induced by anti-UNC5B treatment. The reason for these differences can be explained by the different modes of action of the two antibodies: anti-UNC5B-2 internalizes the receptor and therefore interferes with all UNC5B-dependent pathways (see below), whereas anti-Robo4-1 specifically blocks the interaction with UNC5B. Interestingly, treatment with both antibodies at the same time mimics the anti-UNC5B phenotype, indicating that Robo4 acts upstream of UNC5B. Together with our PAE cell-culture and in vivo permeability data, the corneal pocket experiments therefore support a model where Robo4 activates UNC5B thereby inhibiting VEGFR-induced angiogenic signaling (Figure 7).

Hypervascularization after blocking of UNC5B is also seen in postnatal retinal vessels, confirming and extending our previous reports that UNC5B functions as a negative regulator of developmental angiogenesis (Bouvree et al., 2008; Larrivee et al., 2007; Lu et al., 2004). As deletion of *Robo4* leaves retinal vessels unaffected, we suggest that additional UNC5B ligands may compensate for the absence of Robo4 during developmental angiogenesis. We show that Netrin-1 can mimic Robo4 effects on repulsion of UNC5B expressing cells and Src activation via UNC5B. Deletion of *Ntn-1* also leaves developmental angiogenesis unaffected (G. Strasser and K. Bouvrée, unpublished results). In addition to Robo4 and Netrin-1, UNC5B binds to Netrin-3 and FLRT3, a transmembrane molecule implicated in early mesodermal cell adhesion (Karaulanov et al., 2009; Wang et al., 1999). UNC5B has also been shown to interact with Neogenin and to transduce signals initiated by Netrin-4 and repulsive guidance molecule (RGM) (Hata et al., 2009; Lejmi et al., 2008). Any of these interactions, alone or in combination, may therefore compensate for the absence of Robo4 during developmental angiogenesis. Which combination of UNC5B ligands mediates developmental angiogenesis remains to be determined.

Robo4-UNC5B Interactions Stabilize Vessels

Blocking the Robo4-UNC5B interaction leads to vessel barrier breakdown, indicating that Robo4-UNC5B interactions are required to maintain vessel integrity and prevent vessel leak in vivo. Vessel barrier breakdown after Robo4-UNC5B block can be rescued by a VEGF-trap and the Src inhibitor PP2, supporting the model that UNC5B maintains vessel integrity at least in part by counteracting VEGF-mediated Src kinase activation. Treatment of *Robo4*$^{-/-}$ mice with Robo4 protein rescued vessel barrier function, and soluble Robo4 blocked VEGF-induced permeability in wild-type mice, but not in mice treated with anti-UNC5B-2, indicating that Robo4 mediates vascular stability by binding and signaling through UNC5B. Therefore, interaction between these two receptors in the vasculature is required to

maintain vessel barrier function rather than for guidance processes. Treatment with soluble Robo4 may help restore vascular integrity in diseases characterized by excessive angiogenesis and vascular leak.

EXPERIMENTAL PROCEDURES

Additional methods can be found in the Supplemental Experimental Procedures.

Protein Interaction Screens

An "in-house" library (Clark et al., 2003) of over 1900 purified protein constructs containing Fc or histidine tags was screened for binding to Robo4-Fc with the Octet system (ForteBio) that uses biolayer interferometry to detect binding. Library proteins were stored frozen and diluted into HBS-P buffer (10 mM HEPES [pH 7.4], 0.15 M NaCl and 0.005% [v/v] surfactant P20) for binding screens. Robo4-Fc was loaded to saturation onto anti-human Fc biosensors, then washed in HBS-P buffer for 30 s and placed for 3 min in wells containing library proteins (5 μg/ml) and washed for 30 s. Biosensors were reloaded for 1 min after two interactions. Binding is presented as responses >0.2 nM and an unrelated protein was used in parallel screens to identify unspecific protein binding.

Surface Plasmon Resonance

Binding experiments were carried out by surface plasmon resonance surface plasmon resonance (SPR) measurements on a Biacore 3000 (GE Healthcare) or ProteOn XPR36 (Bio-Rad Laboratories) instrument at 25°C. Slit2-His and UNC5B-Fc were immobilized at high surface densities (~5000 RU) on an activated Biacore CM5 sensor chip using standard amine coupling procedures as described by the manufacturer. Analytes were injected at a flow rate of 5 μl/min and typically at a concentration of 5 μg/ml in HBS-P for 120 s and allowed to dissociate for 240 s. Blank surfaces were used for background corrections. Injections of 10 mM glycine, pH 3.0 at 100 μl/min for 1 min were used to regenerate surfaces between two experiments. For affinity measurements, UNC5B antibodies or UNC5B-Fc were immobilized at low surface densities (500–1000 RU) on an activated ProteOn GLC sensor chip. For kinetic experiments, two-fold serial dilutions of analytes (60 to 1.875 nM for UNC5B-Ig2-His, 200 to 3.125 nM for Robo4-Ig2-His) were injected in phosphate-buffered saline (PBS), 0.005% v/v Tween-20 (pH 7.4) at a flow rate of 80 μl/min and sensorgrams for association and dissociation phases were recorded. Analytes were injected for 300 s and allowed to dissociate for 600 s. Association rates (kon) and dissociation rates (koff) were calculated using a one-to-one Langmuir binding model by simultaneous fitting the association and dissociation sensorgrams (ProteOn Manager, version 2.0, Bio-Rad). The equilibrium dissociation constant (K_D) was calculated as the ratio koff/kon. For binding competition experiments hUNC5B-Fc and UNC5B-His proteins were immobilized at high surface densities (3000–4000 RU) on an activated ProteOn GLC sensor chip. Analytes and 1:1 molar mixtures of analytes were injected in PBS, 0.005% v/v Tween-20 (pH 7.4) at a flow rate of 100 μl/min and sensorgrams for association and dissociation phases were recorded as described above. Data were processed with the ProteOn Manger software (version 2.0, Bio-Rad).

Alkaline Phosphatase and Immunofluorescence Staining

Procedures used for immunolabeling and production of AP-fusion proteins were described (Xu et al., 2010). A full description can be found in the Supplemental Experimental Procedures.

Cell Culture, Fluorescence-Activated Cell Sorting Analysis

A full description of cell culture methods can be found in Supplemental Experimental Procedures. For fluorescence-activated cell sorting (FACS) analysis, PAECs were plated onto 6-well plates in complete Dulbecco's modified Eagle's medium (DMEM). The next day, cells were treated with Netrin-1 (recombinant mouse, 500 ng/ml) or Robo4-Ig2-His (sRobo4) UNC5B-Fc and/or blocking antibodies (100 μg/ml). Cells were detached using Accutase, washed and their fluorescence was analyzed with FACSCalibur cytometer (BD Bioscience). The results represent the percentage of the geometric mean compared to the untreated control of three independent experiments for each condition.

Immunoblotting and Immunoprecipitation

HUAEC (2×10^5) were seeded in 60 mm dishes, cultured for 24 hr in ECGM-2 at 37°C and 5% CO_2. Cells were starved for 12 hr in endothelial basal medium 2 (EBM-2; Promocell) supplemented with 2% FBS, followed by serum-free EBM-2 for 4 hr and treated with Netrin-1 (recombinant mouse, R&D Systems, 500 ng/ml) or sRobo4 (100 μg/ml). Cells were lysed in RIPA buffer (20 mM Tris pH 7.5, 60 mM NaCl, 1% Triton X-100, 0.5% deoxycholic acid, 0.1% sodium dodecyl sulfate, 10% glycerol, 25 mM β-glycerol phosphate, 50 mM sodium fluoride, 2 mM sodium pyrophosphate, 1 mM sodium orthovanadate, and 1× protease inhibitor cocktail, Calbiochem), proteins were separated on sodium dodecyl sulfate polyacrylamide gel electrophoresis and transferred to nitrocellulose membrane (Bio-Rad). Membranes were blocked in TBS, 0.1% Tween 20, 5% bovine serum albumin (BSA) followed by incubation at 4°C overnight with primary antibodies diluted in blocking buffer: anti-Src, anti-phospho-Src (Y418), anti-Erk, anti-phospho-Erk, anti-VEGFR2, p-1175 anti-VEGFR2, anti-VE-Cadherin (all 1:1000, Cell Signaling), anti-UNC5B (0.2 ug/ml, R&D Systems), and anti-phospho-Tyrosine clone 4G10 (1:1000; Upstate). Membranes were washed and incubated with peroxidase-conjugated secondary antibodies (1:2000; Pierce) in blocking buffer for 2 hr at room temperature (RT), and proteins were visualized with enhanced chemoluminescence western blotting detection reagents (Pierce). Membranes were exposed using the Fujifilm LAS-3000 imaging system. PAEC (2×10^6) UNC5B-FL-GFP were seeded in 100 mm diameter dishes and cultured for 24 hr in complete DMEM. Cells were starved overnight in serum-free DMEM and treated with the indicated molecules. Protein extracts were prepared by lysing the cells in NP40-sodium desoxycholate buffer (20 mM Tris pH 7.5, 150 mM NaCl, 0.1% sodium desoxycholate, 0.5% NP40, 10% glycerol, 1 mM β-glycerophosphate, 1 mM NaF, 2.5 mM Na pyrophosphate, 1 mM Na_3VO_4, and 1× protease inhibitor cocktail). Five hundred micrograms of total proteins were immunoprecipitated using anti-Src (1:100; Cell Signaling) or anti-VE-Cadherin antibodies (1:50; Cell Signaling) on G-Sepharose beads (GE Healthcare). Protein separation and immunoblotting were described above.

Generation of Phage Antibodies against UNC5B

Human phage antibody libraries with synthetic diversities in the selected complementary determining regions (H1, H2, H3, L3) were used for panning. The Fab fragments were displayed bivalently on the surface of M13 bacteriophage particles (Lee et al., 2004). MaxiSorp 96-well immunoplates (Nunc) were coated overnight at 4°C with human UNC5B-Fc or human UNC5B-His protein (10 μg/ml) and blocked for 1 hr with 2% milk in PBS. The antibody phage libraries were added and incubated overnight at RT. Plates were washed with PBST, bound phage eluted with 50 mM HCL and 500 mM NaCl for 30 min, and neutralized with equal volume of 1M Tris base. Recovered phages were amplified in *Escherichia coli* XL-1 blue cells. During subsequent selection rounds, the incubation time of the phage antibodies was decreased to 2 hr and the stringency of plate washing was gradually increased (Liang et al., 2007). Phage ELISA and DNA sequencing identified unique and specific phage antibodies binding to UNC5B ECD. Interesting clones were reformatted to full length IgGs by cloning VL and VH regions of individual clones into LPG3 and LPG4 vectors, respectively, for transient expression in mammalian cells.

Mouse Corneal Micropocket Assay

The mouse corneal angiogenesis pocket assay was adapted from Cao et al. (2004). Briefly, hydroxyl methylcellulose and aluminum sucralfate micropellets (0.2 mm × 0.2 mm) containing VEGF-A (175 ng, R&D) were coated with Hydron polymer. CD-1 mice (Charles-River, 12 weeks old) were anesthetized and the Hydron pellet was implanted into the base of a surgically created corneal pocket, positioned 1.0–1.4 mm from the corneal limbus. After implantation, veterinary ophthalmic ointment was applied to the eye. To evaluate the effect of anti-Robo4-1 and anti-UNC5B-2 on VEGF induced angiogenesis in the cornea, animals were injected intraperitoneally (i.p.) on day 0, 2, and 4 with antibodies at 20 mg/kg (anti-VEGF at 5 mg/kg) or with vehicle. After 7 days, animals were sacrificed and the corneas harvested. Vessels were imaged using CD31 (hamster anti-mouse CD31, AbD Serotec) and anti-SMA (Cy-3 anti-SMA, Sigma) antibodies.

Vessel Permeability Assays

For microsphere extravasation, 100 ul of green fluorescent microsphere solution (0.1 um, Duke Scientific) was injected into the tail vein of 6-week-old C57/bl6 wild-type and *Robo4*$^{-/-}$ or mice injected i.p. with anti-UNC5B-1, anti-UNC5B-2 or anti-Robo4-1 (20 mg/kg, daily for 4 days before microsphere injection). Beads were left to circulate for 1 hr, mice were anesthetized (Ketamin/Rompun) and perfused intracardially with 20 ml of 1% PAF in PBS. Retinas (six per condition) were dissected and stained. For Miles assay, the bellies of 6-week-old C57/BL6J *Robo4*$^{+/+}$ or *Robo4*$^{-/-}$ female littermates was shaved and the next day mice were injected intravenously with 100 μl 1% Evan's blue solution. Thirty minutes after injection, 20 μl of PBS containing BSA, VEGFA (R&D, 2.5 μg/ml), sRobo4 (100 μg/ml), Flt1-Fc (R&D, 100 μg/ml), or PP2 (10 μM) with or without blocking antibodies (1 mg/ml) were injected intradermally into two of four treatment zones. Fifteen minutes (VEGF treatments) or 1 hr later (antibody treatments), the animals were sacrificed, and skin punch biopsies were incubated in formamide solution at 56°C for 24 hr to extract the dye. The absorbance of the solution was measured with a spectrophotometer at 620 nm–405 nm. Between 4–10 mice per group were analyzed for each panel in Figures 6B–6G. Data are expressed as fold increase compared to control. Error bars represent standard error of the mean; Mann-Whitney U-test, * $p < 0.05$, ***$p < 0.001$.

SUPPLEMENTAL INFORMATION

Supplemental Information includes Supplemental Experimental Procedures and five figures and can be found with this article online at doi:10.1016/j.devcel.2010.12.001.

ACKNOWLEDGMENTS

This work was supported by grants from Inserm, Agence Nationale de la Recherche, Fondation pour la Recherche Médicale (FRM), Fondation Leducq (Artemis Transatlantic Network of Excellence) and Fondation Bettencourt. T. Mathivet was supported by FRM. B. Larrivée and K. Bouvrée were supported by Association pour la Recherche contre le Cancer. We thank N. Huet, A. Barret, J. Theillon, N. Boggetto, and T. Damerval for their help.

Received: July 27, 2010
Revised: October 25, 2010
Accepted: November 30, 2010
Published: January 18, 2011

REFERENCES

Adams, R.H., and Alitalo, K. (2007). Molecular regulation of angiogenesis and lymphangiogenesis. Nat. Rev. Mol. Cell Biol. *8*, 464–478.

Bouvree, K., Larrivee, B., Lv, X., Yuan, L., DeLafarge, B., Freitas, C., Mathivet, T., Breant, C., Tessier-Lavigne, M., Bikfalvi, A., et al. (2008). Netrin-1 inhibits sprouting angiogenesis in developing avian embryos. Dev. Biol. *318*, 172–183.

Brose, K., Bland, K.S., Wang, K.H., Arnott, D., Henzel, W., Goodman, C.S., Tessier-Lavigne, M., and Kidd, T. (1999). Slit proteins bind Robo receptors and have an evolutionarily conserved role in repulsive axon guidance. Cell *96*, 795–806.

Cao, R., Bjorndahl, M.A., Religa, P., Clasper, S., Garvin, S., Galter, D., Meister, B., Ikomi, F., Tritsaris, K., Dissing, S., et al. (2004). PDGF-BB induces intratumoral lymphangiogenesis and promotes lymphatic metastasis. Cancer Cell *6*, 333–345.

Clark, H.F., Gurney, A.L., Abaya, E., Baker, K., Baldwin, D., Brush, J., Chen, J., Chow, B., Chui, C., Crowley, C., et al. (2003). The secreted protein discovery initiative (SPDI), a large-scale effort to identify novel human secreted and transmembrane proteins: a bioinformatics assessment. Genome Res. *13*, 2265–2270.

Dickson, B.J., and Gilestro, G.F. (2006). Regulation of commissural axon pathfinding by slit and its Robo receptors. Annu. Rev. Cell Dev. Biol. *22*, 651–675.

Eliceiri, B.P., Paul, R., Schwartzberg, P.L., Hood, J.D., Leng, J., and Cheresh, D.A. (1999). Selective requirement for Src kinases during VEGF-induced angiogenesis and vascular permeability. Mol. Cell *4*, 915–924.

Fukuhara, N., Howitt, J.A., Hussain, S.A., and Hohenester, E. (2008). Structural and functional analysis of slit and heparin binding to immunoglobulin-like domains 1 and 2 of Drosophila Robo. J. Biol. Chem. *283*, 16226–16234.

Gavard, J., and Gutkind, J.S. (2006). VEGF controls endothelial-cell permeability by promoting the beta-arrestin-dependent endocytosis of VE-cadherin. Nat. Cell Biol. *8*, 1223–1234.

Hanke, J.H., Gardner, J.P., Dow, R.L., Changelian, P.S., Brissette, W.H., Weringer, E.J., Pollok, B.A., and Connelly, P.A. (1996). Discovery of a novel, potent, and Src family-selective tyrosine kinase inhibitor. Study of Lck- and FynT-dependent T cell activation. J. Biol. Chem. *271*, 695–701.

Hata, K., Kaibuchi, K., Inagaki, S., and Yamashita, T. (2009). Unc5B associates with LARG to mediate the action of repulsive guidance molecule. J. Cell Biol. *184*, 737–750.

Hohenester, E., Hussain, S., and Howitt, J.A. (2006). Interaction of the guidance molecule Slit with cellular receptors. Biochem. Soc. Trans. *34*, 418–421.

Huminiecki, L., Gorn, M., Suchting, S., Poulsom, R., and Bicknell, R. (2002). Magic roundabout is a new member of the roundabout receptor family that is endothelial specific and expressed at sites of active angiogenesis. Genomics *79*, 547–552.

Hussain, S.A., Piper, M., Fukuhara, N., Strochlic, L., Cho, G., Howitt, J.A., Ahmed, Y., Powell, A.K., Turnbull, J.E., Holt, C.E., and Hohenester, E. (2006). A molecular mechanism for the heparan sulfate dependence of Slit-Robo signaling. J. Biol. Chem. *281*, 39693–39698.

Jones, C.A., London, N.R., Chen, H., Park, K.W., Sauvaget, D., Stockton, R.A., Wythe, J.D., Suh, W., Larrieu-Lahargue, F., Mukouyama, Y.S., et al. (2008). Robo4 stabilizes the vascular network by inhibiting pathologic angiogenesis and endothelial hyperpermeability. Nat. Med. *14*, 448–453.

Jones, C.A., Nishiya, N., London, N.R., Zhu, W., Sorensen, L.K., Chan, A.C., Lim, C.J., Chen, H., Zhang, Q., Schultz, P.G., et al. (2009). Slit2-Robo4 signalling promotes vascular stability by blocking Arf6 activity. Nat. Cell Biol. *11*, 1325–1331.

Karaulanov, E., Bottcher, R.T., Stannek, P., Wu, W., Rau, M., Ogata, S., Cho, K.W., and Niehrs, C. (2009). Unc5B interacts with FLRT3 and Rnd1 to modulate cell adhesion in Xenopus embryos. PLoS ONE *4*, e5742.

Kaur, S., Samant, G.V., Pramanik, K., Loscombe, P.W., Pendrak, M.L., Roberts, D.D., and Ramchandran, R. (2008). Silencing of directional migration in roundabout4 knockdown endothelial cells. BMC Cell Biol. *9*, 61.

Kidd, T., Brose, K., Mitchell, K.J., Fetter, R.D., Tessier-Lavigne, M., Goodman, C.S., and Tear, G. (1998). Roundabout controls axon crossing of the CNS midline and defines a novel subfamily of evolutionarily conserved guidance receptors. Cell *92*, 205–215.

Larrivee, B., Freitas, C., Trombe, M., Lv, X., Delafarge, B., Yuan, L., Bouvree, K., Breant, C., Del Toro, R., Brechot, N., et al. (2007). Activation of the UNC5B receptor by Netrin-1 inhibits sprouting angiogenesis. Genes Dev. *21*, 2433–2447.

Lee, C.V., Liang, W.C., Dennis, M.S., Eigenbrot, C., Sidhu, S.S., and Fuh, G. (2004). High-affinity human antibodies from phage-displayed synthetic Fab libraries with a single framework scaffold. J. Mol. Biol. *340*, 1073–1093.

Lejmi, E., Leconte, L., Pedron-Mazoyer, S., Ropert, S., Raoul, W., Lavalette, S., Bouras, I., Feron, J.G., Maitre-Boube, M., Assayag, F., et al. (2008). Netrin-4 inhibits angiogenesis via binding to neogenin and recruitment of Unc5B. Proc. Natl. Acad. Sci. USA *105*, 12491–12496.

Leonardo, E.D., Hinck, L., Masu, M., Keino-Masu, K., Ackerman, S.L., and Tessier-Lavigne, M. (1997). Vertebrate homologues of C. elegans UNC-5 are candidate netrin receptors. Nature *386*, 833–838.

Liang, W.C., Dennis, M.S., Stawicki, S., Chanthery, Y., Pan, Q., Chen, Y., Eigenbrot, C., Yin, J., Koch, A.W., Wu, X., et al. (2007). Function blocking antibodies to neuropilin-1 generated from a designed human synthetic antibody phage library. J. Mol. Biol. *366*, 815–829.

London, N.R., Zhu, W., Bozza, F.A., Smith, M.C., Greif, D.M., Sorensen, L.K., Chen, L., Kaminoh, Y., Chan, A.C., Passi, S.F., et al. (2010). Targeting

Robo4-dependent slit signaling to survive the cytokine storm in sepsis and influenza. Sci. Transl. Med. *2*, 23ra19.

Long, H., Sabatier, C., Ma, L., Plump, A., Yuan, W., Ornitz, D.M., Tamada, A., Murakami, F., Goodman, C.S., and Tessier-Lavigne, M. (2004). Conserved roles for Slit and Robo proteins in midline commissural axon guidance. Neuron *42*, 213–223.

Lu, X., Le Noble, F., Yuan, L., Jiang, Q., De Lafarge, B., Sugiyama, D., Breant, C., Claes, F., De Smet, F., Thomas, J.L., et al. (2004). The netrin receptor UNC5B mediates guidance events controlling morphogenesis of the vascular system. Nature *432*, 179–186.

Marlow, R., Binnewies, M., Sorensen, L.K., Monica, S.D., Strickland, P., Forsberg, E.C., Li, D.Y., and Hinck, L. (2010). Vascular Robo4 restricts proangiogenic VEGF signaling in breast. Proc. Natl. Acad. Sci. USA *107*, 10520–10525.

Morlot, C., Thielens, N.M., Ravelli, R.B., Hemrika, W., Romijn, R.A., Gros, P., Cusack, S., and McCarthy, A.A. (2007). Structural insights into the Slit-Robo complex. Proc. Natl. Acad. Sci. USA *104*, 14923–14928.

Okada, Y., Yano, K., Jin, E., Funahashi, N., Kitayama, M., Doi, T., Spokes, K., Beeler, D.L., Shih, S.C., Okada, H., et al. (2007). A three-kilobase fragment of the human Robo4 promoter directs cell type-specific expression in endothelium. Circ. Res. *100*, 1712–1722.

Park, K.W., Morrison, C.M., Sorensen, L.K., Jones, C.A., Rao, Y., Chien, C.B., Wu, J.Y., Urness, L.D., and Li, D.Y. (2003). Robo4 is a vascular-specific receptor that inhibits endothelial migration. Dev. Biol. *261*, 251–267.

Sheldon, H., Andre, M., Legg, J.A., Heal, P., Herbert, J.M., Sainson, R., Sharma, A.S., Kitajewski, J.K., Heath, V.L., and Bicknell, R. (2009). Active involvement of Robo1 and Robo4 in filopodia formation and endothelial cell motility mediated via WASP and other actin nucleation-promoting factors. FASEB J. *23*, 513–522.

Stein, E., and Tessier-Lavigne, M. (2001). Hierarchical organization of guidance receptors: silencing of netrin attraction by slit through a Robo/DCC receptor complex. Science *291*, 1928–1938.

Suchting, S., Heal, P., Tahtis, K., Stewart, L.M., and Bicknell, R. (2005). Soluble Robo4 receptor inhibits in vivo angiogenesis and endothelial cell migration. FASEB J. *19*, 121–123.

Tang, X., Jang, S.W., Okada, M., Chan, C.B., Feng, Y., Liu, Y., Luo, S.W., Hong, Y., Rama, N., Xiong, W.C., et al. (2008). Netrin-1 mediates neuronal survival through PIKE-L interaction with the dependence receptor UNC5B. Nat. Cell Biol. *10*, 698–706.

Wang, H., Copeland, N.G., Gilbert, D.J., Jenkins, N.A., and Tessier-Lavigne, M. (1999). Netrin-3, a mouse homolog of human NTN2L, is highly expressed in sensory ganglia and shows differential binding to netrin receptors. J. Neurosci. *19*, 4938–4947.

Xu, Y., Yuan, L., Mak, J., Pardanaud, L., Caunt, M., Kasman, I., Larrivée, B., Suchting, S., Del Toro, R., Medvinski, A., et al. (2010). Neuropilin-2 mediates VEGF-C induced lymphatic sprouting together with VEGFR3. J. Cell Biol. *188*, 115–130.

Zhang, B., Dietrich, U.M., Geng, J.G., Bicknell, R., Esko, J.D., and Wang, L. (2009). Repulsive axon guidance molecule Slit3 is a novel angiogenic factor. Blood *114*, 4300–4309.